

Characterization of charged defects in $\text{Cd}_x\text{Hg}_{1-x}\text{Te}$ and CdTe crystals by electron beam induced current and scanning tunneling spectroscopy

G. Panin,^{a)} C. Díaz-Guerra, and J. Piqueras

Departamento de Física de Materiales, Facultad de Físicas, Universidad Complutense, E-28040 Madrid, Spain

(Received 17 November 1997; accepted for publication 26 February 1998)

A correlative study of the electrically active defects of $\text{Cd}_x\text{Hg}_{1-x}\text{Te}$ and CdTe crystals has been carried out using a scanning electron microscope/scanning tunneling microscope (SEM/STM) combined system. Charged structural and compositional defects were revealed by the remote electron beam induced current (REBIC) mode of the scanning electron microscope. The electronic inhomogeneities of the samples were analyzed with nm resolution by current imaging tunneling spectroscopy (CITS) measurements, which showed the existence of built-in electrostatic barriers as well as local variations of the surface band gap in the defect areas imaged by REBIC. © 1998 American Institute of Physics. [S0003-6951(98)01617-9]

The investigation of the local electronic properties of semiconductor materials and devices is a subject of increasing interest related to the progress of microelectronics technology. In particular, the potential application of cadmium based binary and ternary II-VI compounds in optoelectronics (solar energy conversion, infrared detection, etc.) is an active field of research. Several beam injection techniques based in the scanning electron microscope (SEM), like cathodoluminescence and electron beam induced current (EBIC), have provided in the past years space resolved information on structural and compositional defects controlling electrical and optical properties of CdTe and $\text{Cd}_x\text{Hg}_{1-x}\text{Te}$.¹⁻⁴ On the other hand, scanning tunneling microscopy (STM) and spectroscopy allow us to simultaneously investigate both the structural and electronic properties of semiconductors with high resolution. In particular, spatially resolved spectroscopic measurements, as current induced tunneling spectroscopy (CITS),⁵ can be used to construct images that reveal nanometer scale variations in the surface electronic structure of the samples.⁶ Previous STM works on CdTe refer mainly to surface structure observations performed either in ultra-high vacuum (UHV)^{7,8} or in air,⁹ while no STM study on $\text{Cd}_x\text{Hg}_{1-x}\text{Te}$ has been to our knowledge reported. In the present work, the capability of STM and CITS to study local electronic properties of undoped CdTe and $\text{Cd}_x\text{Hg}_{1-x}\text{Te}$ crystals and to correlate them with SEM-EBIC measurements is investigated. Our STM was implemented in a SEM with EBIC detection system. This experimental arrangement enabled us to study the same area of the sample by both techniques, SEM-EBIC and STM-CITS. EBIC images revealed the existence of inhomogeneities in the electronic properties of the samples, which were analyzed in the same region with higher resolution by CITS.

Undoped p -type CdTe ($p = 5 \times 10^{15} \text{ cm}^{-3}$) crystals grown by the Bridgman method, as well as p -type $\text{Cd}_{0.56}\text{Hg}_{0.44}\text{Te}$ crystals ($p = 3 \times 10^{15} \text{ cm}^{-3}$) grown by the solid state recrystallization method were investigated.

Samples were cleaved in air and immediately mounted in the chamber of a SEM/STM combined instrument based on a Leica Stereoscan 440 SEM operating under a vacuum of 1×10^{-6} Torr. Similar SEM/STM combined systems, working in UHV or in high vacuum conditions, have been recently developed and employed in the study of different types of materials.¹⁰⁻¹³ Remote EBIC or REBIC,¹⁴ which has been previously applied to the characterization of II-VI compounds,^{1,15} was also used in this work. For REBIC measurements two Ohmic contacts were provided by Ag paste with Au wires at opposite sides of the samples. EBIC and REBIC signals were detected with a Matelect ISM-5 system. Electrochemically etched or mechanically sharpened Pt-Ir and Au wires were used as STM probe tips. For CITS measurements the topographic height was measured on every point of a 128×128 pixel grid, the feedback loop interrupted for 2 ms, and the voltage digitally ramped from the tunnel voltage to a set of 44 predetermined values while the current was sampled. This provides 44 tunneling current files at different voltages, in addition to the constant current topograph. To analyze the obtained data the normalized differential conductance $[(dI/dV)/(I/V)]$ spectra were used. This quantity removes most of the exponential dependence of tunneling current on tip-sample separation and applied bias voltage,¹⁶ and provides a rather direct measure of the surface density of states.^{17,18}

EBIC and REBIC images revealed the existence of electrically active compositional and structural defects in both semiconductors. Inhomogeneity of the electronic behavior of the samples was mainly related to the presence of subgrain boundaries and precipitates. An example of this inhomogeneity can be appreciated in the REBIC image of a CdTe crystal shown in Fig. 1. Charged defects present in the material act as local potential barriers in which electron-hole pairs generated by the SEM beam are separated. The bright-dark contrast features observed in the micrograph are due to the opposite directions of the electric field on both sides of the defects. This contrast was also observed in the REBIC images of the $\text{Cd}_x\text{Hg}_{1-x}\text{Te}$ crystals which were similar to those previously reported for the same kind of samples.^{19,20}

^{a)}Permanent address: Institute of Microelectronics Technology, Russian Academy of Sciences, 142432, Chernogolovka, Moscow District, Russia.

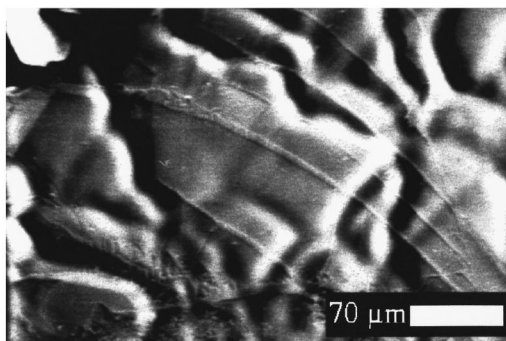


FIG. 1. SEM-REBIC image of electrically active subgrain boundaries in a CdTe crystal (energy and current of the electron beam are 17 keV and 2 nA, respectively).

Due to the capability of our SEM/STM instrument to visualize and select the scanning area of the STM tip, CITS data could be acquired in areas where EBIC or REBIC contrast was found. An example of these observations is presented in Fig. 2, which shows the constant current topography image (a) and the spatially resolved tunneling current signal (CITS images) at selected bias voltages (b)–(d) of a $\text{Cd}_{0.56}\text{Hg}_{0.44}\text{Te}$ crystal. Figure 3 shows a similar measurement in a CdTe sample. Figures 2(a) and 3(a) are representative of the topography of the $\text{Cd}_{0.56}\text{Hg}_{0.44}\text{Te}$ and CdTe crystals, respectively. A fine grain structure is usually revealed in the STM images of $\text{Cd}_{0.56}\text{Hg}_{0.44}\text{Te}$ surfaces, while CdTe crystals show a more uniform topography. In the ternary compound, grain sizes usually range from 1 to 10 nm in width and from 1 to 8 nm in height. However, quite flat areas—separated by steps with a height of about 5–10 nm—were frequently observed in CdTe surfaces. CITS images show that the inhomogeneity of electronic properties revealed by EBIC is also present at a finer scale. Such higher resolution cannot be attained by SEM-based techniques. Figures 2(b)–2(d) show CITS images recorded in $\text{Cd}_{0.56}\text{Hg}_{0.44}\text{Te}$ at sample voltages above and below the 0.64 eV bulk band gap of the crystal. An

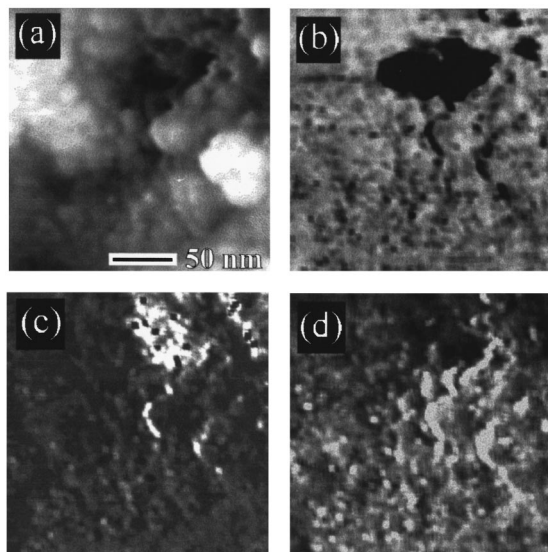


FIG. 2. $200 \times 200 \text{ nm}^2$ STM image of a $\text{Cd}_{0.56}\text{Hg}_{0.44}\text{Te}$ sample. (a) Topography image acquired with a sample voltage of -0.9 V and 0.8 nA tunneling current. Gray-scale range is 18 nm . (b)–(d) Corresponding CITS images obtained at $+1.03 \text{ V}$ (b), -0.98 V (c), and -0.53 V (d) sample voltages.

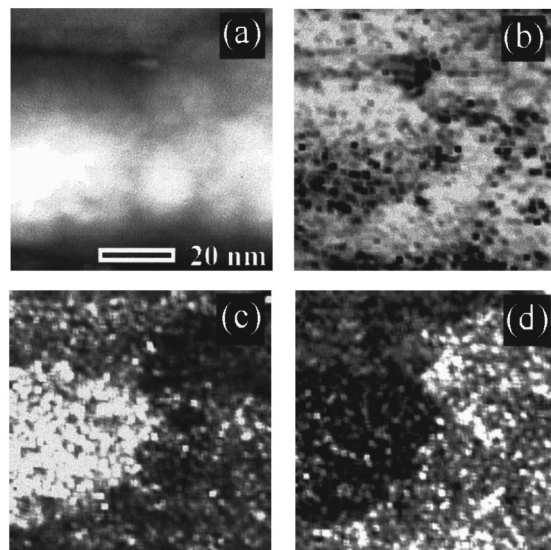


FIG. 3. $70 \times 70 \text{ nm}^2$ STM image of a CdTe crystal. (a) Topography image acquired with -1.8 V sample voltage and 0.88 nA tunneling current. Gray-scale range is 8 nm . (b)–(d) Corresponding CITS images acquired at $+0.98 \text{ V}$ (b), -0.98 V (c), and -2 V (d) sample voltages.

enhanced contrast can be appreciated in the CITS images corresponding to several localized—nm sized—grains and some intergrain regions. CITS contrast related to local conductance variations is also observed in CdTe samples at voltages below [Figs. 3(b) and 3(c)] and above [Fig. 3(d)] the band gap value of 1.5 eV . Both native point and extended defects, as well as impurities, are usually electrically active in $\text{Cd}_x\text{Hg}_{1-x}\text{Te}$ and CdTe semiconductors. In the case of $\text{Cd}_x\text{Hg}_{1-x}\text{Te}$, compositional inhomogeneities are related to the weakness of Hg bonding in the lattice and the high mobility of the Hg atoms, which migrate from or towards the surface creating positively charged interstitials or negatively charged vacancies.²¹ CITS images acquired in both semiconductors can be explained if surface nonstoichiometry induces defect states that significantly increase the midgap electron density contributing to the appreciable tunneling current observed at low applied bias voltages. Our CITS results were found to be reproducible in measurements performed on different samples, under different tunneling conditions and with different probe tips. The main features of the associated $(dI/dV)/(I/V)$ spectra were also observed in those corresponding to static $I-V$ characteristics that were recorded for comparison. These normalized conductance spectra provide further information on the samples inhomogeneity. As an example, Fig. 4 shows spectra of a $\text{Cd}_{0.56}\text{Hg}_{0.44}\text{Te}$ crystal obtained from different positions inside a region where a charged subgrain boundary was revealed by REBIC, as well as a spectrum recorded outside that region. Each curve of Fig. 4 was plotted from the data set of the corresponding CITS file by selecting small areas of about $12 \times 12 \text{ nm}^2$ on which data were averaged, and actually represents the average of about 15 individual curves. Spectrum (a), which corresponds to an area far from the boundary, shows the Fermi level (zero bias voltage) close to the valence band edge followed by a gap of about 0.6 eV as the bias is increased to positive values, in agreement with both the p -type conduction and the bulk band gap of the sample. Spectra acquired in the defect area [(b) and (c)] show a narrower surface band

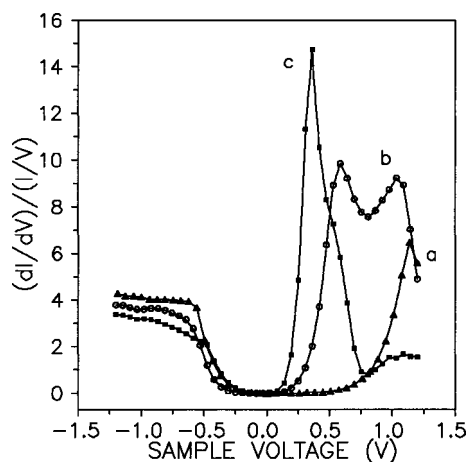


FIG. 4. Normalized differential conductance spectra acquired on a $\text{Cd}_{0.56}\text{Hg}_{0.44}\text{Te}$ sample outside (a) and inside, (b) and (c), an area of bright-dark REBIC contrast associated to a charged subgrain boundary.

gap. Conductance curves showing reduced gaps were recorded in all the regions containing charged defects that we examined. This included several areas of at least three different subgrain boundaries of each sample. However, the measured gap widths were found to depend on the boundary considered and the position along the defect where they were acquired. Curve (b) shows, in addition, a shift of the Fermi level towards the conduction band edge, which agrees with the REBIC detection of a built-in electrostatic barrier at the defect. This shift was never observed in curves recorded far from the charged subgrain boundaries. Regarding spectrum (c), the width of the low conductance region in this curve can be estimated to be about 0.3 eV. This value compares with the 0.32 eV band gap of Te precipitates that were observed in EBIC images of this semiconductor and also detected by wavelength dispersive x-ray microanalysis performed on the crystals. These results show that the electronic inhomogeneities revealed in the SEM-EBIC and REBIC images are also detected in the conductance spectra, with strong variations in surface band gap which would be related to nanoscaled clustering or precipitation processes.

In summary, a combined SEM/STM system has been used to study the electrically active defect structure of $\text{Cd}_x\text{Hg}_{1-x}\text{Te}$ and CdTe crystals on two different scales. Local variations of surface band gap were revealed with nm resolution by STM-CITS in the regions where charged compositional and structural defects were detected by SEM-EBIC and REBIC.

This work was supported by DGICYT (Project PB93-1256) and by CICYT (Project IN93-0012). The help of Professor A. M. Baró, Dr. A. Asenjo, and Dr. J. Gómez-Herrero is gratefully acknowledged. G. Panin thanks Spanish MEC for a research grant.

- ¹G. Panin and E. Yakimov, *Semicond. Sci. Technol.* **7A**, 150 (1992).
- ²U. Pal, P. Fernández, J. Piqueras, N. V. Sochinskii, and E. Dieguez, *J. Appl. Phys.* **78**, 1992 (1995).
- ³G. Panin, P. Fernández, and J. Piqueras, *Semicond. Sci. Technol.* **11**, 1354 (1996).
- ⁴A. Castaldini, A. Cavallini, B. Fraboni, L. Polenta, P. Fernández, and J. Piqueras, *Phys. Rev. B* **54**, 7622 (1996).
- ⁵R. J. Hamers, R. M. Tromp, and J. E. Demuth, *Phys. Rev. Lett.* **56**, 1972 (1986).
- ⁶R. M. Feenstra, *Surf. Sci.* **299/300**, 965 (1994).
- ⁷L. Seehofer, G. Falkenberg, R. L. Johnson, V. H. Etgens, S. Tatarenko, D. Brun, and B. Daudin, *Appl. Phys. Lett.* **67**, 1680 (1995).
- ⁸L. Seehofer, V. H. Etgens, G. Falkenberg, M. B. Veron, D. Brun, B. Daudin, S. Tatarenko, and R. L. Johnson, *Surf. Sci.* **347**, L55 (1996).
- ⁹R. Castro-Rodríguez, M. Zapata-Torres, A. Zapata-Navarro, A. I. Oliva, and J. L. Peña, *J. Appl. Phys.* **79**, 184 (1996).
- ¹⁰P. M. Thibado, Y. Liang, and D. A. Bonnell, *Rev. Sci. Instrum.* **65**, 3199 (1994).
- ¹¹A. Asenjo, A. Buendía, J. M. Gómez-Rodríguez, and A. M. Baró, *J. Vac. Sci. Technol. B* **12**, 1658 (1994).
- ¹²R. J. N. Coopes, T. Tiedje, S. L. Konsek, and T. P. Pearsall, *Ultramicroscopy* **68**, 257 (1997).
- ¹³A. Asenjo, J. M. Gómez-Rodríguez, and A. M. Baró, *Ultramicroscopy* **42-44**, 933 (1992).
- ¹⁴L. O. Bubulac and W. E. Tennant, *Appl. Phys. Lett.* **52**, 1255 (1988).
- ¹⁵D. B. Holt, B. Raza, and A. Wojcik, *Mater. Sci. Eng., B* **42**, 14 (1996).
- ¹⁶J. A. Strosio, R. M. Feenstra, and A. P. Fein, *Phys. Rev. Lett.* **57**, 2579 (1986).
- ¹⁷N. D. Lang, *Phys. Rev. B* **34**, 5947 (1986).
- ¹⁸R. M. Feenstra, J. A. Strosio, and A. P. Fein, *Surf. Sci.* **181**, 295 (1987).
- ¹⁹G. N. Panin and E. B. Yakimov, *J. Phys. (Paris), Colloq.* **C6**, 181 (1991).
- ²⁰G. N. Panin, *Inst. Phys. Conf. Ser.* **134**, 743 (1993).
- ²¹Y. Nemirovsky and G. H. Bahir, *J. Vac. Sci. Technol. A* **7**, 206 (1989).